Enantiomerically enriched, polycrystalline molecular sieves

Stephen K. Brand[a], Joel E. Schmidt[a,b], Michael W. Deem[c,d], Frits Daeyaert[c,d], Yanhang Ma[e], Osamu Terasaki[e,f], Marat Orazov[a,g], and Mark E. Davis[a,1]

[a]Chemical Engineering, California Institute of Technology, Pasadena, CA 91125; [b]Debye Institute for Nanomaterials Science, Utrecht University, 3584 CG Utrecht, The Netherlands; [c]Department of Bioengineering, Rice University, Houston, TX 77005; [d]Department of Physics & Astronomy, Rice University, Houston, TX 77005; [e]School of Physical Science and Technology, ShanghaiTech University, Shanghai 201210, China; [f]Department of Materials & Environmental Chemistry, Stockholm University, Stockholm SE-10691, Sweden; and [g]Chemical Engineering, Stanford University, Stanford, CA 94305

Contributed by Mark E. Davis, April 3, 2017 (sent for review March 21, 2017; reviewed by Avelino Corma and Alexander Katz)

Zeolite and zeolite-like molecular sieves are being used in a large number of applications such as adsorption and catalysis. Achievement of the long-standing goal of creating a chiral, polycrystalline molecular sieve with bulk enantioenrichment would enable these materials to perform enantioselective functions. Here, we report the synthesis of enantiomerically enriched samples of a molecular sieve. Enantiopure organic structure directing agents are designed with the assistance of computational methods and used to synthesize enantioenriched, polycrystalline molecular sieve samples of either enantiomer. Computational results correctly predicted which enantiomer is obtained, and enantiomeric enrichment is proven by high-resolution transmission electron microscopy. The enantioenriched and racemic samples of the molecular sieves are tested as adsorbents and heterogeneous catalysts. The enantioenriched molecular sieves show enantioselectivity for the ring opening reaction of epoxides and enantioselective adsorption of 2-butanol (the R enantiomer of the molecular sieve shows opposite and approximately equal enantioselectivity compared with the S enantiomer of the molecular sieve, whereas the racemic sample of the molecular sieve shows no enantioselectivity).

chirality | zeolite | asymmetric catalysis | chiral adsorption

The synthesis of zeolites and zeolite-like molecular sieves has been accomplished using organic structure-directing agents (OSDAs) (1–4). This synthetic method uses an organic molecule (OSDA) to interact with and influence the assembly pathway of the inorganic components to create a crystalline, organic–inorganic composite material. Upon removal of the OSDA, the microporous void space that is created can be exploited in a variety of applications (i.e., catalysis, separations, ion exchange, and adsorption) (5). These microporous, polycrystalline materials are 3D networks of oxide tetrahedra [zeolites contain only silicon and aluminum, whereas zeolite-like molecular sieves can have a broader range of elements (1–5)] that create highly ordered, hydrothermally stable framework structures with pores of sizes less than 2 nm. Molecular sieves provide shape-selective properties and, coupled with the inclusion of catalytic active sites, are capable of innumerable highly selective chemical reactions. Despite the abundance of chirality in nature, the discovery of a zeolite or zeolite-like microporous material with enantioselective properties has remained elusive. Enantioenriched, chiral zeolitic materials are of particular interest for their potential to provide robust, new, enantiospecific, shape-selective catalytic pathways and separation processes (6–13).

Several inherently chiral molecular sieves have been synthesized to date (although the bulk, polycrystalline samples are racemic), including *BEA, CZP, GOO, -ITV, JRY, LTJ, OSO, SFS, and STW [molecular sieve framework types are designated by three-letter codes that define the unique connectivity of the oxide tetrahedral (14)]. In particular, several studies have reported polymorph A (which possesses a chiral helical pore) enriched *BEA. However, zeolite *BEA is limited in that the material crystallizes as highly faulted intergrowths of a racemic mixture of polymorph A and polymorph B (achiral). In 1992, Davis and Lobo (15) discussed the concept of synthesizing a chiral *BEA molecular sieve via the use of a chiral OSDA and reported low enantioenrichment (ee) for both a chemical reaction and an adsorption experiment. Recently, Tong et al. (16) have reported a high-fluoride method of synthesizing polymorph A enriched *BEA using achiral OSDAs (although it is difficult to understand the origin of the proposed enantioenrichment) and reported low ee's from a chemical reaction. Other authors have reported samples enriched in polymorph A with similar ambiguity in enantioenrichment (17–20). These studies suggest the viability of synthesizing an enantioenriched, chiral molecular sieve. However, the inherent difficulty in controlling the synthesis of polymorphic domains, and the enantiomeric domains of only polymorph A in *BEA, has made it very problematic to conclusively prove that a bulk sample of a molecular sieve does in fact have an enantiomerically enriched framework content. Davis and Lobo (15) discussed this issue and suggested that a preferred approach would be to design syntheses that target chiral molecular sieve structures where individual crystals are single enantiomorphs (microporous analogs to quartz). The STW framework is an example of this type of molecular sieve; recent evidence shows that each individual crystal is a single enantiomorph (i.e., there are no polymorph or opposite enantiomeric domains within a single crystal) (21).

A molecular sieve with the STW framework was initially synthesized as a germanosilicate (denoted SU-32) in 2008 (22) and then as a hydrothermally stable pure-silica material in 2012 (23).

Significance

Zeolites and zeolite-like molecular sieves are used as adsorbents and heterogeneous catalysts to prepare a wide variety of products ranging from gasoline to monomers for polymers such as polyethylene terephthalate, which is used in plastic bottles. Pharmaceuticals, pesticides, fragrances, and components in food can contain chiral centers. Here, we prepare enantioenriched polycrystalline samples of a molecular sieve and show that this type of porous material can function as an adsorbent to separate chiral molecules and as a heterogeneous catalyst to perform chiral reactions. This initial demonstration proves that bulk, enantioenriched chiral zeolites and zeolite-like molecular sieves can be synthesized and that this type of solid can be used to prepare chiral, small molecules.

Author contributions: S.K.B., J.E.S., M.W.D., F.D., Y.M., O.T., M.O., and M.E.D. designed research; S.K.B., J.E.S., Y.M., and M.O. performed research; S.K.B., J.E.S., M.W.D., Y.M., O.T., M.O., and M.E.D. analyzed data; S.K.B., J.E.S., and M.E.D. wrote the paper; and M.W.D. and F.D. performed computational work.

Reviewers: A.C., Instituto de Tecnología Química (UPV-CSIC); and A.K., University of California, Berkeley.

The authors declare no conflict of interest.

Freely available online through the PNAS open access option.

[1]To whom correspondence should be addressed. Email: mdavis@cheme.caltech.edu.

This article contains supporting information online at www.pnas.org/lookup/suppl/doi:10.1073/pnas.1704638114/-/DCSupplemental.

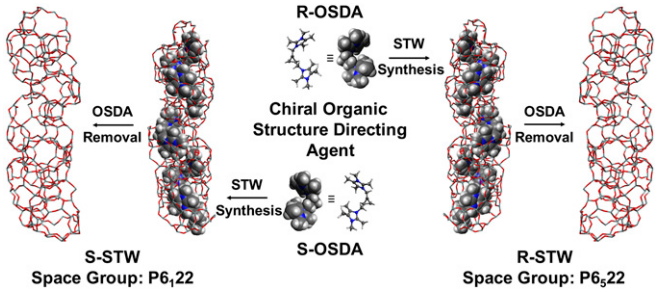

Fig. 1. Illustration of the synthesis of enantioenriched STW samples using enantiopure, chiral OSDAs.

The STW structure contains 10-membered rings (MRs, the number of oxygen or tetrahedral atoms that make up the ring) that form chiral helical pores (22). Past synthesis protocols that used achiral OSDAs resulted in bulk, polycrystalline samples that were racemic mixtures of the two structural enantiomers. STW, therefore, provides a good model for designing the synthesis of bulk, polycrystalline samples of either the "R" or "S" enantiomers of the framework. Here, we use computational methods to aid in our design of chiral OSDAs for the synthesis of enantioenriched STW and show that a bulk sample of a polycrystalline, molecular sieve can be synthesized with significant enantiomeric enrichment. Our design (shown in Fig. 1) provides for the synthesis of either the R or the S enantiomers of STW, thus yielding materials that enable appropriate control experiments when elucidating structures and functions.

Results and Discussion

Directed Computational Design of a Chiral OSDA for STW. Schmidt et al. (24) reported on the synthesis of STW using a computationally predicted OSDA. This work demonstrated the feasibility of a priori predicting chemically synthesizable monoquaternary, imidazolium OSDAs to create a specified, fluoride-mediated, pure-silica framework. Additionally, STW has been reported to form using diquaternary imidazolium-based OSDAs that are of sufficient size to conform to 10MR channel structure, implying more rigid, chiral analogs may be included in the framework of STW, and may potentially impart structural chirality (24–28). Here, we implemented the previously published computational method implemented by Schmidt et al. (24) and Pophale et al. (29) and used the molecular design constraints suggested by Davis and Lobo (15). The computational method was modified such that a given enantiomer of each potential OSDA molecule was simulated in both enantiomers of STW, with successful candidates producing a strong stabilization in only a single enantiomer. Based on our previous work with STW, we believed that a computed stabilization energy larger than −15 kJ·(mol Si)$^{-1}$ would be needed to form STW. Ultimately, a single OSDA candidate was selected (Table 1). Relative to the other predicted OSDAs for STW, **2** has the largest energy difference between enantiomers, making it the most suitable target for experimental evaluation. Coupled with energy predictions, this molecule was also selected after ensuring that the both enantiomers were synthetically attainable (24). A full description of the computational method is provided in *SI Appendix*.

Synthesis and Characterization of Enantiopure OSDA 2. Detailed procedures for the chiral resolution and reaction schemes used to synthesize OSDA **2** are given in *SI Appendix*, Figs. S1 and S2. Chiral resolution of the starting compound (*trans*-2-phenylcyclopropane-1-carboxylic acid, 1) was performed by successive crystallizations with either dehydroabietylamine or quinine as chiral derivatization agents to obtain the R (1a) or S (1a′) forms of the starting material (*SI Appendix*, Fig. S1). Polarimetry measurements were taken for the salt and free-acid forms of 1a and 1a′ to confirm enantiopurity, after the separation was complete. Further details of the synthesis of **2** are provided in *SI Appendix* (note: enantiomers of **2** will be denoted R-**2** and S-**2**). (Λ,*R*)-BINPHAT tetrabutylammonium salt was used as a chiral shift reagent to detect the enantiopurity of **2** after executing the reactions outlined in *SI Appendix*, Fig. S2. As shown in Fig. 2, the neat product ^{1}H NMR resonances at δ 4.80 and 4.04 ppm are singular and distinct multiplets. Addition of BINPHAT to a racemic sample of **2** results in a twofold spectral change: (*i*) a distinct shift upfield of only the aforementioned peaks from their initial position and (*ii*) an observed peak split. Integration of the split peaks indicates that they maintain a 1:1 ratio, expected for a racemic compound. However, the two enantiomers of **2** show only a single peak. This method confirms the enantiopurity of **2** and demonstrates that no racemization occurs throughout the organic synthesis scheme.

Synthesis and Characterization of Enantioenriched STW. Syntheses of STW were conducted with enantiopure samples of the R and S enantiomers of **2**, as well as the racemic mixture of the two. These syntheses were performed at temperatures and H_2O/SiO_2 ratios that are typical for silica-enriched, fluoride-mediated syntheses. Because STW is composed of ∼80% double four-tetrahedral atom rings that are known to be stabilized by inclusion of germanium, addition of varying quantities of germanium to the synthesis gels was explored (30, 31). Following the work of Schmidt et al. (24), reagent molar ratios that led to the synthesis of STW in the shortest times were 1 SiO_2:x GeO_2:5 H_2O:0.5 HF:0.5 **2** at 160 °C (where x varies from 0.05 to 0.5) using 10% (wt/wt) seeds produced from an achiral diquaternary OSDA with crystal sizes on the order of 1 μm. Aluminum-containing samples were also synthesized (in the presence of Ge) using aluminum isopropoxide. In these syntheses, initial gel Si/Al ratios were maintained above 50; otherwise, RTH impurities were observed in the resultant products (25). Aging the synthesis gels over the course of 24 h was found to reduce crystallization times. A complete summary of the synthesis results is provided (*SI Appendix*, Tables S1–S3) along with representative powder X-ray diffraction (PXRD) patterns (*SI Appendix*, Fig. S3). Additionally, ^{19}F, ^{29}Si, and ^{27}Al solid-state NMR (SS NMR) spectra, a representative thermogravimetric analysis, and a selection of scanning electron micrographs are listed as supporting

Table 1. Potential chiral OSDAs including 2, which was used to prepare enantioenriched STW, and their associated stabilization energies in both enantiomers of the STW framework (stabilization energies in kilojoules per mole Si)

Proposed OSDA	$E_{enantiomer\ 1}$ (i.e., $P6_122$)	$E_{enantiomer\ 2}$ (i.e., $P6_522$)
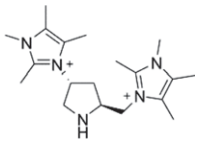	−16.32	−14.60
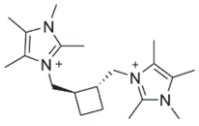	−14.65	−1.37
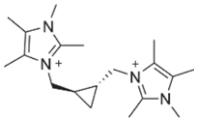	−15.27	−1.58

Molecule in third row: OSDA **2**.

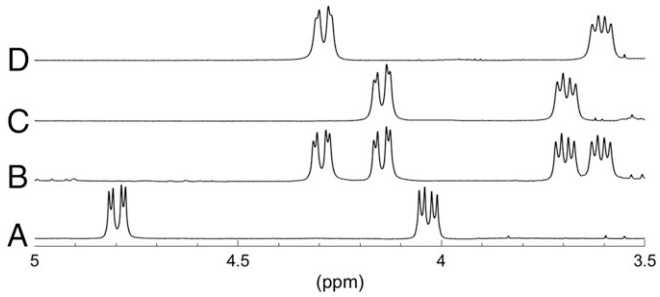

Fig. 2. The ^{1}H NMR chiral shift experiments to analyze the enantiopurity of **2**: (*A*) neat racemic **2**, (*B*) racemic **2** with BINPHAT, (*C*) R-**2** with BINPHAT, and (*D*) S-**2** with BINPHAT. An imidazole methyl resonance in *A* has been suppressed at δ 3.74 ppm for clarity.

characterizations (*SI Appendix*, Figs. S4–S8). In general, the concentrations of germanium and aluminum were found to increase in the product materials relative to the synthesis gel. Representative results from energy-dispersive X-ray spectroscopy are given in *SI Appendix*, Table S4 for products from germanosilicate and aluminogermanosilicate synthesis gels. In addition to STW, numerous other phases were produced without significant variation in synthesis conditions, including LTA, RTH, IWV, CSV, as well as several phases that could not be identified or consisted of layered organosilicate materials. Synthesis of these microporous materials is not unexpected, because they have all been shown to be derived from similarly shaped imidazole-based OSDAs under crystallization conditions similar to those reported here (25–28, 32).

As-made STW crystals obtained using **2** were analyzed by ^{13}C cross-polarization magic-angle spinning SS NMR to evaluate whether the OSDA remains intact and directs the formation of STW. Fig. 3 compares the neat OSDA liquid ^{13}C NMR spectrum (Fig. 3*A*) with those obtained from analyzing the occluded organic (from SS ^{13}C NMR) and the organic recovered by dissolution of the framework structure (liquid ^{13}C NMR). Agreement between all spectra indicates that **2** is occluded intact within the STW framework and is the structure-directing agent. As such, STW is not formed from an organic decomposition product or as a consequence of spontaneous, directed crystallization from the seed crystals. Efforts to perform chiral shift experiments on recovered OSDA **2** collected from dissolution of the STW framework by hydrofluoric acid were not successful due to solubility issues (**2**, chiral shift reagent, and solvent combinations).

Although it has been speculated that chiral OSDAs (when directed toward a chiral structure) should necessarily lead to an enrichment in the chirality of framework, this concept has never been conclusively proven. To do so, the chirality of the organic occluded within the STW structure must be known, as must the chirality of the framework structure for a bulk, polycrystalline sample. CD provides an effective method of accomplishing the former for as-made STW samples. The results for R-, S-, and racemic STW samples are given in Fig. 4. As shown by the data provided in Fig. 4, the molecules occluded within R- and S-STW absorb light at 242 nm with equal and opposite polarities. No measured rotation of light is observed for the racemic sample because, statistically, any polarization effects are negated for a sample containing equivalent quantities of chiral crystals. These data collectively demonstrate that **2** remains chiral and enantiopure within the STW framework. Although it may be possible to analyze the structural chirality of a calcined STW structure, no adsorption in the 200- to 300-nm range was detected from our germanosilicate samples. Incorporation of UV-active heteroatoms beyond those that have been used in this work may provide a pathway for future investigation via CD studies.

In previous reports involving the enrichment of polymorph A in *BEA (which does not guarantee enantioenrichment), characterization of any true structural enrichment of polymorph A has been limited to transmission electron microscopy (TEM) analysis (PXRD analyses are fraught with problems) of the polymorph domains and demonstration of enantioenrichment by measuring some function (e.g., catalysis or adsorption) (15, 16). A distinct issue with this methodology, however, is that the synthesis of these materials lacks proper controls with regard to the enantiomorphs obtained in the product materials, and therefore it is not possible to perform appropriate analytical and experimental controls to confirm chirality. The methods we have developed and used here are not subject to these problems. We are able to control the synthesis of a chiral OSDA (and obtain the R-, S-, and racemic forms thereof) to yield bulk, polycrystalline STW samples composed of individual crystals of a single chirality. As such, characterization and functional results that are capable of probing the bulk chirality of the two enantioenriched samples of opposing direction must demonstrate enantiomeric excess (ee) that is approximately equal and opposite, with the racemic preparation revealing no ee. The CD experiments for the R-, S-, and racemic STW samples provide an illustration of how these types of controls can be exploited to derive meaningful conclusions.

Characterization of the structural chirality of STW is complicated. An examination of the literature yields few methods for effectively determining this property for siliceous microporous materials beyond the demonstration of enantiomeric excesses derived from reactions or adsorption experiments. Analytical difficulty partially stems from the small crystal sizes (as is the case for STW synthesized with OSDAs used here) that prohibit the use of single-crystal XRD. Rojas et al. (31) point toward the possibility of examining the optical activity to quantify enantiomeric excess within a bulk, polycrystalline sample. SEM and high-resolution TEM (HRTEM) have proven to be highly advantageous methods for analyzing crystallite morphologies. HRTEM has been used previously to analyze the polymorph domains in *BEA (16, 20). However, specific chiral space groups (i.e., structural enantiomers) within the detected polymorph A domains were not able to be determined. Fundamentally, the difficulty in unequivocally distinguishing between the space groups of a chiral material using traditional TEM techniques arises from properties inherent to both structural chirality and experimental limitations. Specifically, on a given 2D plane (as is observed in a typical TEM experiment) the structures of the two enantiomers are superimposable and indistinguishable. A method was therefore developed to perform 3D HRTEM experiments by Ma et al. (21) to effectively characterize chiral space groups. The projection of the STW framework shifts after rotation along the

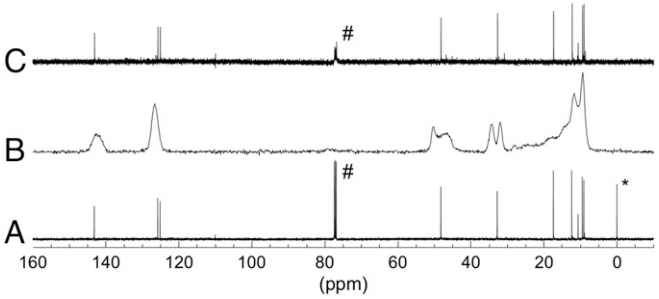

Fig. 3. Comparison of the ^{13}C NMR collected for (*A*) the neat organic, (*B*) the occluded organic within an enantioenriched STW sample, and (*C*) the OSDA recovered dissolving the framework with hydrofluoric acid and extracting the organic. Peaks marked with the symbols # or * denote the $CDCl_3$ solvent and TMS standard, respectively.

CHEMISTRY

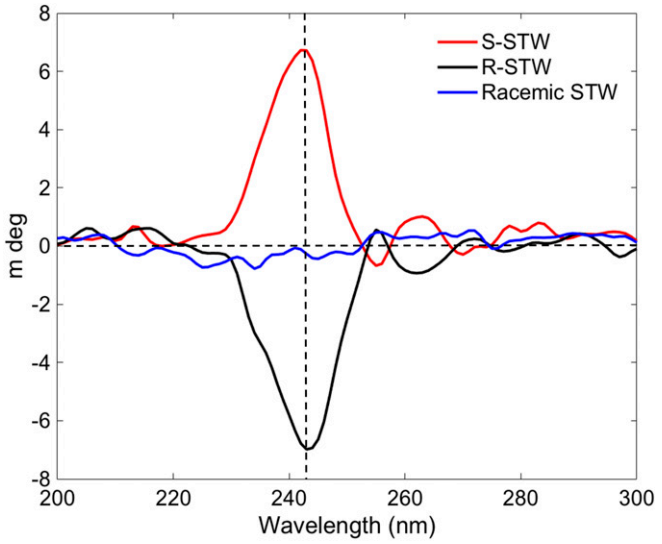

Fig. 4. CD spectra for as-made samples of STW using R-, S-, and racemic OSDA **2**.

screw axis as schematically illustrated in Fig. 5*A*. The rotation direction can be either clockwise (to the right) or counterclockwise (to the left). A zeolite crystal [that has been deposited with gold nanoparticles (diameter ~5 nm) that serve as reference points with the microporous structure] is first aligned to [$2\bar{1}\bar{1}0$] zone axis and a through-focus series of HRTEM images are taken from a thin area. The crystal is then tilted continuously to the right or to the left by 30° about the screw axis. Upon rotation, the [$1\bar{1}00$] zone axis is observed if the tilting is clockwise. Based on simulated results, the crystal is right-handed if the shift direction is downward (Fig. 5 *B* and *C*). Upon rotation, the [$1\bar{1}00$] or [$10\bar{1}0$] zone axes are observed if the tilting direction is to the right or left, respectively. A series of through-focus images are then taken again along either zone axis. Two images along [$2\bar{1}\bar{1}0$] and [$1\bar{1}00$] are obtained by structure projection reconstructions using the through-focus series of HRTEM images and are aligned based on the positions of gold nanoparticles (Fig. 5 *D*–*G* and *SI Appendix*, Figs. S9–S11). By comparing the aligned images from the two zone axes there is an observable shift between the two projections from which the space group of the crystal can be assigned. Additional images are provided in *SI Appendix*.

The results collected from using this method to analyze STW crystals selected from bulk, polycrystalline samples synthesized using the R-, S-, and racemic versions of **2** are given in Table 2. Out of the six crystals analyzed for both the R- and S-OSDA–derived samples, five were determined to possess the $P6_122$ and $P6_522$ space groups, respectively, demonstrating (within this dataset) notable enantioenrichment. Moreover, these experimental results are consistent with computational predictions whereby R-OSDA **2** is expected to yield crystals with $P6_122$ space group and, similarly, S-OSDA **2** is anticipated to result in crystals with the $P6_522$ space group (Table 1). Analysis of the racemic sample resulted in an equal number of crystals from each space group, as expected.

Ideally, for a given sample synthesized using a chiral OSDA, HRTEM analysis would subsequently demonstrate only crystals from the expected space group. However, as shown in Table 2, a crystal from both chiral OSDA-derived samples was determined to be from the unexpected space group (e.g., $P6_522$ from the R-OSDA). Possible reasons for incomplete purity include that (*i*) the crystal of the opposite space group was a seed crystal, (*ii*) there was OSDA degradation that occurred that yielded a racemic portion of the polycrystalline sample, and (*iii*) the inherent nature of the crystallization process does not synthesize an enantiopure, but only an enantioenriched, polycrystalline sample. Although currently the number of crystals that have been analyzed is not sufficient to draw a statistically conclusive picture of the bulk chirality of the samples, these HRTEM data (coupled with the distinct differences detected between R- and S-OSDA synthesized materials) are useful to demonstrate enantioenrichment of a bulk, polycrystalline sample of a molecular sieve.

CD and HRTEM characterizations demonstrate that a given enantiomer of OSDA **2** maintains its respective chirality in the occluded state and is capable of producing an enantioenriched, molecular sieve framework. Although there may exist crystallization processes wherein achiral molecules lead to enantioenrichment of product solids, such as by spontaneous chiral symmetry breaking by self-catalyzed crystallization (33), such systems would not allow for the directed synthesis of specific enantiomers of crystals, as we are able to demonstrate in this work. Thus, it follows that the initial hypothesis by Davis and Lobo (15) that any bulk, polycrystalline sample having enantioenrichment (not obtained solely from chiral

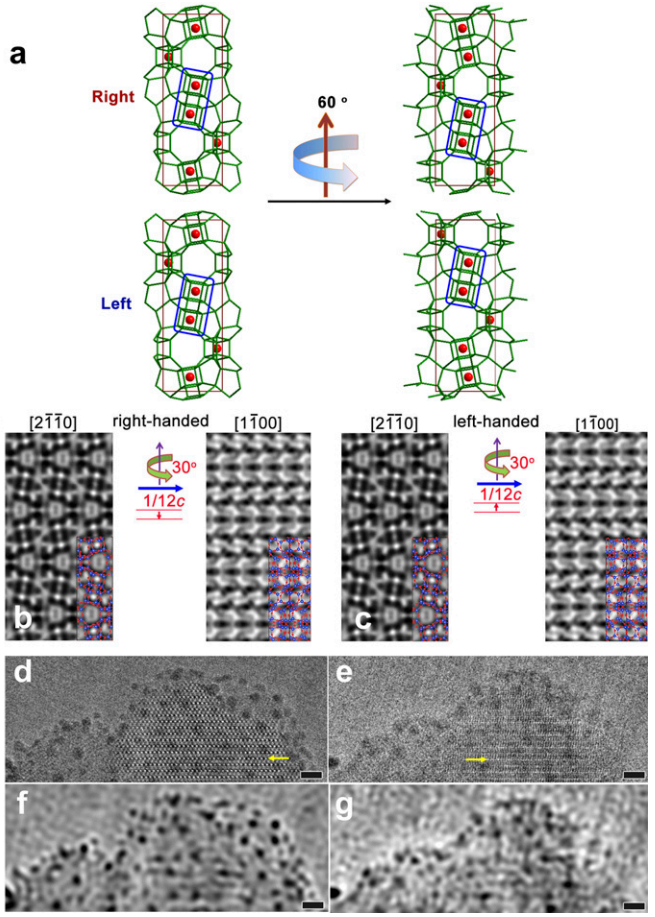

Fig. 5. (*A*) Schematic representation of a sixfold rotation of STW frameworks with different handedness. (*B* and *C*) Simulated HRTEM images of the zeolite with right- and left-handedness, respectively. The atomic structure models, where blue and red balls represent Si and O atoms, were overlaid on top of the simulated images. The shift between two images for right-handed and left-handed STW frameworks has the same length but reverse directions. (*D* and *E*) Comparison of two HRTEM images with gold nanoparticles as markers. A crystal was tilted from [$2\bar{1}\bar{1}0$] (d) to [$10\bar{1}0$] (e) and a shift down was observed, which indicates a space group of $P6_522$. (*F* and *G*) The processed images of *D* and *E* after Fourier filtering that only includes spatial frequencies within a particular range to enhance the contrasts of gold nanoparticles. (Scale bars, 5 nm.)

Table 2. Summary of the results obtained from rotational HRTEM analysis for STW crystals synthesized from the R-, S-, and racemic OSDA 2

OSDA used	No. of crystals analyzed	$P6_122$	$P6_522$
R-**2**	6	5	1
S-**2**	6	1	5
Racemic **2**	6	3	3

seeds) must be derived from a chiral OSDA with a particular set of properties seems valid. Additionally, this synthesis methodology ensures that all forms (R-, S-, and racemic) are attainable, thus allowing for appropriate controls to be performed.

Adsorption and Catalysis with Enantioenriched STW. The chirality in STW is defined over the specific distance within the helical STW pore structure (Fig. 1) (34). As a consequence, adsorption and catalysis that show ee's will involve molecules that are of sufficient size to effectively experience the chirality of the structure, yet still be able to pass through the limited size of the pores. As such, we expect that any measured ee's will be greatly dependent on the selection of molecules used to test for a function. Moreover, the external surfaces of the crystallites may behave nonspecifically, resulting in diminishing ee's.

To examine whether the enantioenriched STW samples are capable of performing enantioselective functions, catalysis and adsorption experiments were conducted. Epoxide ring-opening reactions on 1,2-epoxyalkanes were selected for catalysis, because they have been shown to take place within molecular sieves at relatively low temperatures (35–37). Such low-temperature probe reactions are particularly desirable because symmetry-breaking dispersive interactions with the catalyst surface are expected to be relatively large contributors to the transition state free energies compared with high-temperature scenarios. Reaction and analysis procedures are detailed in *SI Appendix*. The results from these reactions are reported in Table 3. For epoxides shorter than C_8, enantiomeric excesses that are not significantly different from experimental error are observed. However, as the chain length is further extended (to approximate the size of OSDA **2**) the magnitude of the ee's become significantly different from experimental error. Results show that approximately the same magnitude of the ee's are obtained, but in opposite directions, from the R-STW and the S-STW, as should be. *Trans*-stilbene oxide was also used as a substrate and minimal ring opening was observed. Because this substrate is too large to enter the pores of STW, this control experiment demonstrates that the rate of reaction outside the pore structure (i.e., on the surface of the crystals) is negligible, and that any measured ee's do not occur as a consequence of surface or solvent effects. No reactions were observed using uncalcined racemic STW.

Vaporsorption experiments were performed using the pure R-, S-, and racemic solutions of 2-butanol. Previous computational studies suggested that germanosilicate STW is capable of selectively adsorbing R- and S-glycidol into the helices of the respective enantiomers of the framework, with increasing discrimination between enantiomers from a racemic mixture with decreasing system temperatures (38). Experiments were therefore performed at 278 K (which allows for a vapor pressure great enough to collect sufficient adsorption data). Fig. 6 illustrates the adsorption isotherms obtained for R-, S-, and racemic 2-butanol in germanosilicate R- and S-STW. For R-STW, R-2-butanol is selectively adsorbed relative to S-2-butanol. The racemic 2-butanol isotherm lies at the approximate average of the isotherms from the enantiomerically enriched sample 2-butanol isotherms. An equivalent, but inverse, result is observed from S-STW.

Summary

We have computationally designed large, rigid, and stable chiral OSDAs to synthesize the two polycrystalline, enantiomorphs of STW (enantiomerically enriched) following the synthesis heuristics specified by Davis and Lobo (15) for chiral molecular sieves. Under typical silica-enriched, fluoride-mediated inorganic reaction conditions the chiral OSDA directs toward the formation of the STW framework. Solid-state NMR and CD characterizations demonstrate that the occluded OSDA remains intact within the STW pores and retains enantiopurity. Newly developed 3D HRTEM techniques are applied to determine the chirality of individual crystals. These data show that the samples synthesized using a chiral OSDA are enantioenriched with the space group of STW that is a priori computationally predicted based on the OSDA's chirality, whereas the racemic OSDA leads to a racemic mixture of crystals. Thus, we report and confirm the rational and controlled synthesis of bulk, polycrystalline molecular sieve with enantioenrichment. Additionally, we find that the enantioenriched materials are capable of yielding enantioenrichment for reaction and adsorption experiments.

The initial discovery of transition-metal–catalyzed asymmetric reactions by Noyori and coworkers (39) gave preliminary ee's up to 10% for the copper-catalyzed cyclopropanations of olefins. Improvements over time of this catalytic system have to led to industrial applications of asymmetric hydrogenation catalysts (40). We hope that our initial demonstration of

Table 3. Summary of enantiomeric excess from the ring opening of 1,2-epoxyalkanes with methanol using aluminum-containing racemic, R-, and S-STW as catalysts

	Enantiomeric excess of products using enantioenriched STW					
	R-STW		Racemic STW		S-STW	
Substrate	**a**, %	**b**, %	**a**, %	**b**, %	**a**, %	**b**, %
1,2-epoxybutane	–0.14	2.31	0.05	0.06	0.02	–2.26
1,2-epoxyhexane	1.29	2.83	0.20	–0.92	–1.96	–3.46
1,2-epoxyoctane	4.13	9.85	1.14	–0.86	–4.41	–10.65

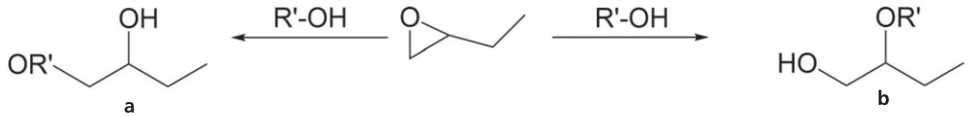

Product **a** is the less-substituted 1-methoxyalkan-2-ol product, and product **b** is the more-substituted 2-methoxyalkan-1-ol product. The reaction solutions were analyzed after 48 h.

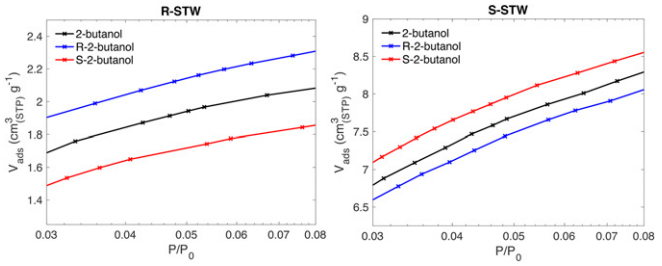

Fig. 6. The 2-butanol adsorption isotherms at 278 K for germanosilicate R- and S-STW. Differences in uptake are a result of variations in sample crystallinity.

molecular sieve asymmetric catalysis may follow a similar pathway.

Materials and Methods

Reagents, OSDA Synthesis, and Characterization. A full list of chemicals used in this study and their sources can be found in *SI Appendix*. The full synthesis procedure for the chiral SDA used in this study as well as the respective ^{1}H and ^{13}C NMR characterization data are described in detail in *SI Appendix*.

STW Synthesis. The hydrothermal synthesis procedures are given in *SI Appendix*, along with a comprehensive list of starting material composition ranges and the resultant products.

HRTEM Sample Preparation. The powdered sample was crushed and dispersed into ethanol using ultrasonic processing. Several drops of the dispersion were dropped onto a carbon-film–supported TEM grid. Gold particles were deposited onto the sample through sputter coating.

Image Collection. Electron diffraction patterns and HRTEM images were obtained using a 200 kV using JEOL JEM-2100F (Cs = 0.5 mm, Cc = 1.1 mm). Each projection image was reconstructed from a through-focus series of 20 HRTEM images acquired with a constant focus step of 53 Å. The structure projection reconstruction was done using software Qfocus (41).

Catalytic Reaction Analysis. In a typical epoxide ring opening reaction, 20 mmol of an epoxide-functionalized substrate and 5 g of methanol (as a nucleophilic solvent) were added to 20 mg of Al-containing STW (Si/Al = 30 ± 10). Reactions were carried out at 323 K in thick-walled crimp-sealed glass reactors (VWR) submerged in a temperature-controlled oil bath. The enantiomeric excess of aliquots was determined by chiral gas chromatography. Detailed descriptions of procedures followed during reaction testing can be found in *SI Appendix*.

ACKNOWLEDGMENTS. S.K.B. thanks Dr. Sonjong Hwang (Caltech) for his assistance with solid-state NMR data collection, Dr. Jay Winkler (Caltech) for assistance with the solid-state circular dichroism experiments, and Dr. Stacey I. Zones (Chevron). Y.M. thanks Peter Oleynikov (ShanghaiTech) for many useful discussions, and ShanghaiTech University for startup funding to support this work. We thank the Chevron Energy and Technology Company for proving funding for the work that was performed at Caltech. This work was also supported by Department of Energy Basic Sciences Grant DE-FG02-03ER15456 (to M.W.D. and F.D.).

1. Moliner M, Rey F, Corma A (2013) Towards the rational design of efficient organic structure-directing agents for zeolite synthesis. *Angew Chem Int Ed Engl* 52:13880–13889.
2. Zones SI (2011) Translating new materials discoveries in zeolite research to commercial manufacture. *Microporous Mesoporous Mater* 144:1–8.
3. Li J, Corma A, Yu J (2015) Synthesis of new zeolite structures. *Chem Soc Rev* 44: 7112–7127.
4. Wang Z, Yu J, Xu R (2012) Needs and trends in rational synthesis of zeolitic materials. *Chem Soc Rev* 41:1729–1741.
5. Čejka J, Corma A, Zones S, eds (2010) *Zeolites and Catalysis: Synthesis, Reactions and Applications* (Wiley, New York).
6. Bravo-Suárez JJ, Chaudhari RV, Subramaniam B (2013) Design of heterogeneous catalysts for fuels and chemicals processing: An overview. *Novel Materials for Catalysis and Fuels Processing*. ACS Symposium Series, eds Bravo-Suárez JJ, Kidder MK, Schwartz V (American Chemical Society, Washington, DC), pp 3–68.
7. Corma A, Iglesias M, del Pino C, Sanchez F (1991) New rhodium complexes anchored on modified USY zeolites. A remarkable effect of the support on the enantioselectivity of catalytic hydrogenation of prochiral alkenes. *J Am Chem Soc* 18:1253–1255.
8. Carmona A, Corma A, Iglesias M, Sánchez F (1996) Synthesis and characterisation of chiral Cu(I) complexes of substituted pyrrolidine ligands. Efficient catalysts for cyclopropanation reactions. *Inorg Chim Acta* 244:239–245.
9. Xu ZX, Ma YL, Zhang J (2016) Enantiopure anion templated synthesis of a zeolitic metal-organic framework. *Chem Commun (Camb)* 52:1923–1925.
10. Wang C, Zheng M, Lin W (2011) Asymmetric catalysis with chiral porous metal–organic frameworks: Critical issues. *J Phys Chem Lett* 2:1701–1709.
11. Coronas J (2010) Present and future synthesis challenges for zeolites. *Chem Eng J* 156:236–242.
12. Yu J, Xu R (2008) Chiral zeolitic materials: Structural insights and synthetic challenges. *J Mater Chem* 18:4021–4030.
13. Maier NM, Franco P, Lindner W (2001) Separation of enantiomers: Needs, challenges, perspectives. *J Chromatogr A* 906:3–33.
14. IZA (2017) IZA Structure Commission. Available at www.iza-structure.org.
15. Davis ME, Lobo RF (1992) Zeolite and molecular sieve synthesis. *Chem Mater* 4:756–768.
16. Tong M, et al. (2015) Synthesis of chiral polymorph A-enriched zeolite Beta with an extremely concentrated fluoride route. *Sci Rep* 5:11521.
17. Takagi Y, Komatsu T, Kitabata Y (2008) Crystallization of zeolite beta in the presence of chiral amine or rhodium complex. *Microporous Mesoporous Mater* 109:567–576.
18. Taborda F, Willhammar T, Wang Z, Montes C, Zou X (2011) Synthesis and characterization of pure silica zeolite beta obtained by an aging-drying method. *Microporous Mesoporous Mater* 143:196–205.
19. Camblor MA, Corma A, Valencia S (1996) Spontaneous nucleation and growth of pure silica zeolite-B free of connectivity defects. *Chem Commun (Camb)* (20):2365–2366.
20. Zhang G, Wang B, Zhang W, Li M, Tian Z (2016) Synthesis of polymorph A-enriched beta zeolites in a HF-concentrated system. *Dalton Trans* 45:6634–6640.
21. Ma Y, Oleynikov P, Terasaki O (2017) Electron-crystallography approaches for determining the handedness of a chiral zeolite nano-crystal. *Nat Mater*, in press.
22. Tang L, et al. (2008) A zeolite family with chiral and achiral structures built from the same building layer. *Nat Mater* 7:381–385.
23. Rojas A, Camblor MA (2012) A pure silica chiral polymorph with helical pores. *Angew Chem Int Ed Engl* 51:3854–3856.
24. Schmidt JE, Deem MW, Davis ME (2014) Synthesis of a specified, silica molecular sieve by using computationally predicted organic structure-directing agents. *Angew Chem Int Ed Engl* 53:8372–8374.
25. Schmidt JE, Deimund MA, Davis ME (2014) Facile preparation of aluminosilicate RTH across a wide composition range using a new organic structure-directing agent. *Chem Mater* 26:7099–7105.
26. Schmidt JE, Xie D, Rea T, Davis ME (2015) CIT-7, a crystalline, molecular sieve with pores bounded by 8 and 10-membered rings. *Chem Sci (Camb)* 6:1728–1734.
27. Boal BW, et al. (2015) Facile synthesis and catalysis of pure-silica and heteroatom LTA. *Chem Mater* 27:7774–7779.
28. Schmidt JE, Chen C-Y, Brand SK, Zones SI, Davis ME (2016) Facile synthesis, characterization, and catalytic behavior of a large-pore zeolite with the IWV framework. *Chemistry* 22:4022–4029.
29. Pophale R, Daeyaert F, Deem MW (2013) Computational prediction of chemically synthesizable organic structure directing agents for zeolites. *J Mater Chem A Mater Energy Sustain* 1:6750–6760.
30. Sastre G, Pulido A, Corma A (2005) An attempt to predict and rationalize relative stabilities and preferential germanium location in Si/Ge zeolites. *Microporous Mesoporous Mater* 82:159–163.
31. Rojas A, Arteaga O, Kahr B, Camblor MA (2013) Synthesis, structure, and optical activity of HPM-1, a pure silica chiral zeolite. *J Am Chem Soc* 135:11975–11984.
32. Boal BW, et al. (2016) Synthesis of germanosilicate molecular sieves from mono- and di-quaternary ammonium OSDAs constructed from benzyl imidazolium derivatives: Stabilization of large micropore volumes including new molecular sieve CIT-13. *Chem Mater* 28:2158–2164.
33. Kondepudi DK, Kaufman RJ, Singh N (1990) Chiral symmetry breaking in sodium chlorate crystallizaton. *Science* 250:975–976.
34. Dryzun C, Mastai Y, Shvalb A, Avnir D (2009) Chiral silicate zeolites. *J Mater Chem* 19: 2062–2069.
35. Onaka M, Kawai M, Izumi Y (1985) Zeolite-catalyzed ring-opening of epoxides with amines. *Chem Lett* 14:779–782.
36. Ogawa H, Miyamoto Y, Fujigaki T, Chihara T (1996) Ring-opening of 1,2-epoxyalkane with alcohols over H-ZSM-5 in liquid phase. *Catal Lett* 40:253–255.
37. Tang B, et al. (2014) Improved postsynthesis strategy to Sn-Beta zeolites as Lewis acid catalysts for the ring-opening hydration of epoxides. *ACS Catal* 4:2801–2810.
38. Zhang L, Jiang J (2011) Enantioselective adsorption and diffusion of S-/R-glycidol in homochiral zeolites: A molecular simulation study. *J Membr Sci* 367:63–70.
39. Nozaki H, Moriuti S, Takaya H, Noyori R (1966) Asymmetric induction in carbenoid reaction by means of a dissymmetric copper chelate. *Tetrahedron Lett* 7:5239–5244.
40. Noyori R (2002) Asymmetric catalysis: Science and opportunities (Nobel lecture). *Angew Chem Int Ed Engl* 41:2008–2022.
41. Wan W, Hovmöller S, Zou X (2012) Structure projection reconstruction from through-focus series of high-resolution transmission electron microscopy images. *Ultramicroscopy* 115:50–60.